

Supporting information

Cryo-generated Ferrous-superoxo Porphyrin: EPR, Resonance Raman and DFT studies

Takehiro Ohta,^{a,b,*} Jin-Gang Liu,^{b,c,*} Perumandla Nagaraju,^b
Takashi Ogura^a and Yoshinori Naruta^{b,d,*}

^a *Picobiology Institute, Graduate School of Life Science, University of Hyogo, Hyogo 679-5148, Japan.*

Email: takehiro@sci.u-hyogo.ac.jp

^b *Institute for Materials Chemistry and Engineering, Kyushu University, Fukuoka 812-8581, Japan.*

^c *Department of Chemistry, East China University of Science and Technology, 20237 Shanghai,
China.*

Email: liujingang@ecust.edu.cn

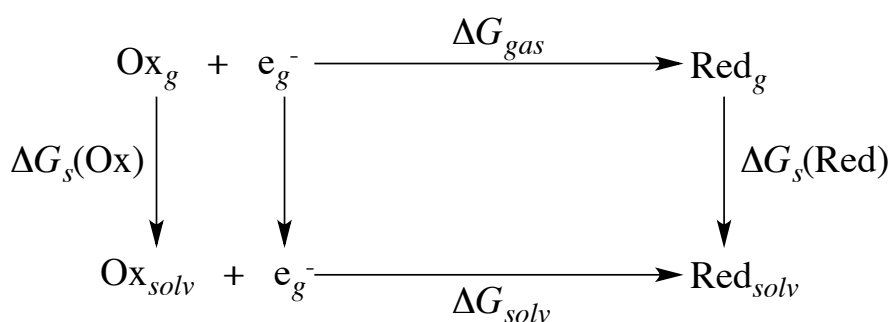
^d *Institute of Science and Technology Research, Chubu University, Kasugai, Aichi 487-8501, Japan.*

Email: naruta@isc.chubu.ac.jp

Materials and cryo-reduction. The model complex $[\text{Fe}^{\text{II}}(\text{TMPIm})]$ and its oxy-form $[(\text{TMPIm})\text{Fe}^{\text{III}}(\text{O}_2^{\cdot-})]$ were prepared as previously described.¹ The oxyform of the sample was prepared in a quartz NMR tube (5.0φ x 380L mm) with a concentration ca.1.5 mM. The tube was immersed in liquid N_2 and reduced by γ -irradiation with a ^{60}Co source [185TBq (5000Ci)] to a dose of ca. 300 kGy. During the γ -ray irradiation experiment, we occasionally stopped the irradiation and monitored the progress of reaction using resonance Raman and EPR spectroscopies, and optimized irradiation time. Several duplicated samples were placed in liquid N_2 dewar for cryoradiolytic reduction. During all subsequent operations, the samples were kept fully immersed in liquid N_2 .

Physical methods. EPR spectra were obtained at 77 K in a 5.0-mm diameter EPR quartz tube using a JEOL JES-TE 300 spectrometer. The magnetic field was calibrated using the signal of Mn(II) ion doped in MgO powder ($g = 2.034$ and 1.981). Experimental conditions: microwave frequency: 100 kHz, modulation amplitude: 10 G, and microwave power: 1.0 mW. rR spectra were obtained on a SpectraPro-300i spectrometer (Acton Research) with a 2400-groove grating, a holographic Supernotch filter (Kaiser Optical Systems), and LN-1100PB CCD detector (Princeton Instruments) cooled with liquid N_2 . Spectra were collected at an excitation wavelength (λ_{ex}) of 429.6 nm using a custom-made SHG laser to irradiate a spinning frozen sample positioned with backscattering geometry. The sample was prepared in a quartz NMR tube kept in liquid N_2 in a double-walled low-temperature quartz Dewar flask. Power at the sample was adjusted to less than 5 mW. Peak frequencies were calibrated relative to toluene and CCl_4 standards (accurate to $\pm 1 \text{ cm}^{-1}$). For each rR sample, EPR spectra were also obtained before and after the rR measurement to confirm the absence of any photochemical damage of the sample.

Computational details. DFT computations were carried out using Gaussian 09 program.² Fully optimized molecular structures were obtained by geometry optimization at the B3LYP/6-311+G* (Fe, N, and O_2) and 6-31G* (Other atoms) level. The complex **1** was calculated in a broken symmetry method, in which α and β electron densities are allowed to localize on different atoms. Frequency analyses and solvation energy calculations using PCM model were carried out on the optimized structures using the same theory level.



Scheme 1. Born-Haber cycle.

The calculation of redox potential of molecules relies on free energy change between the reactant and one-electron oxidized or reduced species under solvated conditions. The frequently used procedure to calculate free energy change under solvation

assumes Born-Haber cycle (Scheme 1), in which gas phase free energy change in redox reaction is first calculated and then the gas-phase energy is calibrated by the difference of solvation energy between the reactant and product as shown in equation 1 and 2.

$$\Delta G(aq) = \Delta G(g) + \Delta G_{sol}(Red) - \Delta G_{sol}(Ox) \quad (\text{eq. 1})$$

$$\Delta G(g) = \Delta H(g) - T\Delta S(g) \quad (\text{eq. 2})$$

$$\Delta G(aq) = -nFE^\circ \quad (\text{eq. 3})$$

In our calculations Ox_g corresponds to the gas phase geometry optimized structure of ferric-superoxy heme, and Red_g is one-electron reduced species of Ox_g in gas phase (Scheme 2). The Nernst equation determines the standard one-electron redox potentials, E°/V , as shown in equation 3, where F is the Faraday constant $23.06 \text{ kcal mol}^{-1} \text{ V}^{-1}$. Calculations were carried out for gas-phase geometries employing dielectric constant of 7.6 (Tetrahydrofuran) for the solvating continuum medium. To correlate the computationally obtained redox potential with experimental data, referencing the calculated value with the standard hydrogen electrode potential is necessary, for which 4.43 eV is used.³

Calculation of pK_a is based on the equations 4-6. In equation 5, T corresponds to room temperature 298.15 K and k_B is the Boltzmann constant. The free energy change $\Delta G_a(aq)$ due to the protonation of heme-bound O_2 in aqueous solution was computed by using half reaction of the Born-Haber cycle shown in Scheme 2.

$$\Delta G_a(aq) = \beta pK_a \quad (\text{eq. 4})$$

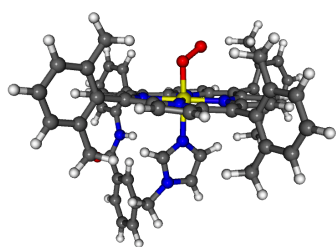
$$\beta = k_B T \quad (\text{eq. 5})$$

$$\Delta G_{aq}(aq) = \Delta G_{aq}(g) + \Delta G_{sol}(A^-) + \Delta G_{sol}(H^+) - \Delta G_{sol}(HA) \quad (\text{eq. 6})$$

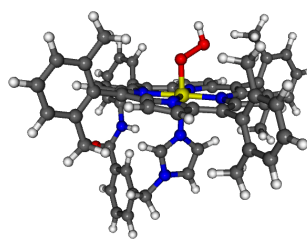
where the $\Delta G_a(g) = \Delta H_a(g) - T\Delta S_a(g)$ is the free energy change due to the protonation in the gas phase, with an enthalpy change $\Delta H_a(g) = \Delta H(\text{DFT}) + \Delta H_{\text{ZPE}}$. The solvation free energy of proton used was -266 kcal/mol .⁴

Table S1. DFT calculated energies (units in hartree).

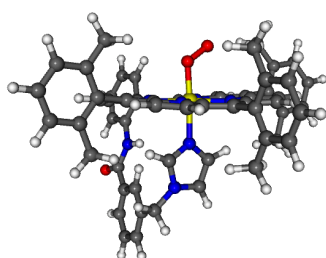
	H(gas)	G(gas)	ZPE	H(sol)	G(sol)
1	-4226.67565310	-4225.813141	0.961028	-4226.69817287	-4225.835661
2	-4226.731082	-4225.871251	0.958245	-4226.795528	-4225.935697
2'	-4226.702252	-4225.846426	0.955448	-4226.770724	-4225.914897
3	-4227.08189738	-4226.210244	0.970895	-4227.13113232	-4226.259479
4	-4227.29431675	-4226.422441	0.971803	-4227.31603508	-4226.444159

**1 (S=0)**

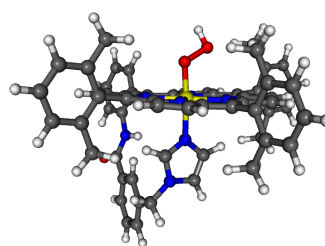
Fe-O: 1.874 Å
O-O: 1.349 Å
Fe-N_{lm}: 2.075 Å
Fe-N_{por}: 2.016 Å (average)

**3 (S=0)**

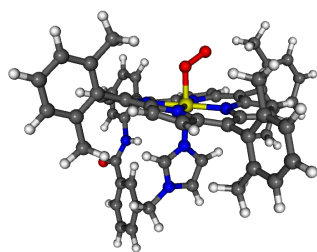
Fe-O: 1.810 Å
O-O: 1.512 Å
Fe-N_{lm}: 2.052 Å
Fe-N_{por}: 2.019 Å (average)

**2 (S=1/2)**

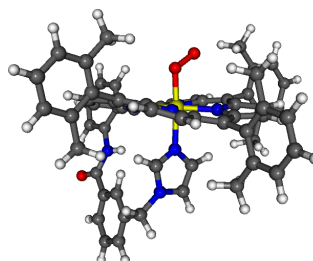
Fe-O: 1.929 Å
O-O: 1.374 Å
Fe-N_{lm}: 2.062 Å
Fe-N_{por}: 2.030 Å (average)

**4 (S=1/2)**

Fe-O: 1.921 Å
O-O: 1.361 Å
Fe-N_{lm}: 2.059 Å
Fe-N_{por}: 2.015 Å (average)

**2' (S=1/2)**

Fe-O: 1.921 Å
O-O: 1.361 Å
Fe-N_{lm}: 2.059 Å
Fe-N_{por}: 2.015 Å (average)

**2' (S=3/2)**

Fe-O: 1.919 Å
O-O: 1.361 Å
Fe-N_{lm}: 2.060 Å
Fe-N_{por}: 2.013 Å (average)

Figure S1. Molecular structure and spin densities of optimized molecular structures 1-4.

Table S2. B3LYP DFT calculated energies (free energies) in doublet, quartet and sextet spin states.

	Ferric-superoxo porphyrin radical anion	Ferrous-superoxo neutral porphyrin
doublet	-4226.70225245 (-4225.846426)	-4226.73108169 (-4225.871251)
quartet	-4226.70283319 (-4225.847746)	-4226.72014260 (-4225.867565)
sextet	-4226.64829401 (-4225.793445)	-4226.71075312 (-4225.860013)

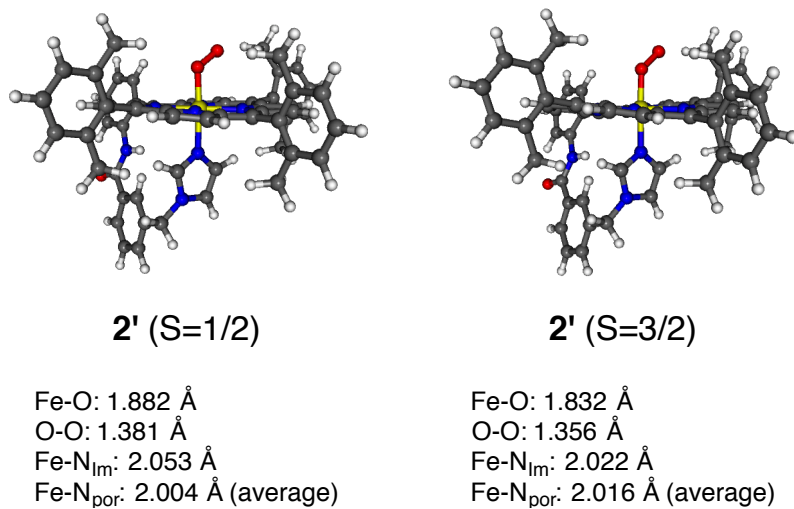


Figure S2. BP86 DFT optimized molecular structures.

Table S3. BP86 DFT calculated spin densities in the doublet, quartet spin states.

	Fe	^p O	^d O	C α	C β	C m	N _{por}
doublet	0.03	0.39	0.50	0.02	0.02	0.02	0.01
quartet	0.99	0.48	0.58	0.16	0.25	0.25	0.06

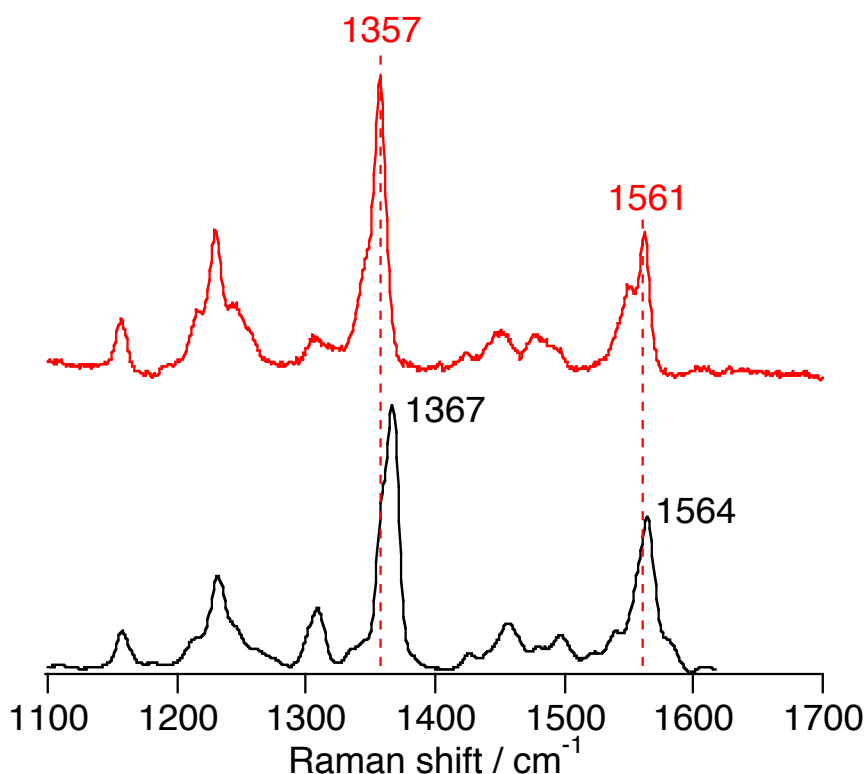


Figure S3. High-frequency rR spectra of the ferric-superoxy species $[(\text{TMPIm})\text{Fe}^{\text{III}}(\text{O}_2^{\bullet})]$ in 20% MeCN/2MeTHF containing $^{16}\text{O}_2$ before (black line) ($\lambda_{\text{ex}} = 413.1$ nm, 77 K, 5 mW) and after (red line) γ -ray irradiation at 77 K ($\lambda_{\text{ex}} = 429.6$ nm, 77 K, 5 mW).

References

- 1 J. -G. Liu, T. Ohta, S. Yamaguchi, T. Ogura, S. Sakamoto, Y. Maeda and Y. Naruta, *Angew. Chem. Int. Ed.*, 2009, **48**, 9262–9267.
- 2 Computations were carried out using Gaussian 09, Revision D.01, M. J. Frisch, G. W. Trucks, H. B. Schlegel, G. E. Scuseria, M. A. Robb, J. R. Cheeseman, G. Scalmani, V. Barone, B. Mennucci, G. A. Petersson, H. Nakatsuji, M. Caricato, X. Li, H. P. Hratchian, A. F. Izmaylov, J. Bloino, G. Zheng, J. L. Sonnenberg, M. Hada, M. Ehara, K. Toyota, R. Fukuda, J. Hasegawa, M. Ishida, T. Nakajima, Y. Honda, O. Kitao, H. Nakai, T. Vreven, J. A. Montgomery, Jr., J. E. Peralta, F. Ogliaro, M. Bearpark, J. J. Heyd, E. Brothers, K. N. Kudin, V. N. Staroverov, R. Kobayashi, J. Normand, K. Raghavachari, A. Rendell, J. C. Burant, S. S. Iyengar, J. Tomasi, M. Cossi, N. Rega, J. M. Millam, M. Klene, J. E. Knox, J. B. Cross, V. Bakken, C. Adamo, J. Jaramillo, R. Gomperts, R. E. Stratmann, O. Yazyev, A. J. Austin, R. Cammi, C. Pomelli, J. W. Ochterski, R. L. Martin, K. Morokuma, V. G. Zakrzewski, G. A. Voth, P. Salvador, J. J. Dannenberg, S. Dapprich, A. D. Daniels, Ö. Farkas, J. B. Foresman, J. V. Ortiz, J. Cioslowski and D. J. Fox, Gaussian, Inc., Wallingford CT, 2009.
- 3 H. Reiss, A. Heller, *J. Phys. Chem. A*, 1985, **89**, 4207-4213.
- 4 E. J. Sundstrom, X. Yang, V. S. Thoi, H. I. Karunadasa, C. J. Chang, J. R. Long, M. Head-Gordon, *J. Am. Chem. Soc.*, 2012, **134**, 5233-5242.